Tokamak Plasma High Field Side Response to an $n = 3$ Magnetic Perturbation: A Comparison of 3D Equilibrium Solutions from Seven Different Codes

A. Reiman[1], N.M. Ferraro[2], A. Turnbull[2], J.K. Park[1], A. Cerfon[3], T.E. Evans[2], M.J. Lanctot[2], E.A. Lazarus[4], Y. Liu[5], G. McFadden[6], D. Monticello[1], Y. Suzuki[7]

[1]*Princeton Plasma Physics Laboratory, Princeton, NJ 08543 USA*
[2]*General Atomics, P.O. Box 85608, San Diego, California 92186-5608, USA*
[3]*New York University, New York, NY, USA*
[4]*Oak Ridge National Laboratory, Oak Ridge, TN, USA*
[5]*EURATOM/CCFE Fusion Association, Culham Science Centre, Abingdon, Oxon, UK*
[6]*National Institute of Standards and Technology, Gaithersburg, MD, USA*
[7]*National Institute for Fusion Science, Kyoto, Japan*

Abstract

In comparing equilibrium solutions for a DIII-D shot that is amenable to analysis by both stellarator and tokamak 3D equilibrium codes, a significant disagreement has been seen between solutions of the VMEC stellarator equilibrium code and solutions of tokamak perturbative 3D equilibrium codes. The source of that disagreement has been investigated, and that investigation has led to new insights into the domain of validity of the different equilibrium calculations, and to a finding that the manner in which localized screening currents at low order rational surfaces are handled can affect global properties of the equilibrium solution. The perturbative treatment has been found to break down at surprisingly small perturbation amplitudes due to overlap of the calculated perturbed flux surfaces, and that treatment is not valid in the pedestal region of the DIII-D shot studied. The perturbative treatment is valid, however, further into the interior of the plasma, and flux surface overlap does not account for the disagreement investigated here. Calculated equilibrium solutions for simple model cases and comparison of the 3D equilibrium solutions with those of other codes indicate that the disagreement arises from a difference in handling of localized currents at low order rational surfaces, with such currents being absent in VMEC and present in the perturbative codes. The significant differences in the global equilibrium solutions associated with the presence or absence of very localized screening currents at rational surfaces suggests that it may be possible to extract information about localized currents from appropriate measurements of global equilibrium plasma properties. That would require improved diagnostic capability on the high field side of the tokamak plasma, a region difficult to access with diagnostics.

I. Introduction

We have been comparing equilibrium solutions for a DIII-D shot that is amenable to analysis by both stellarator and tokamak 3D equilibrium codes, and in that context we have encountered a significant disagreement between solutions of the VMEC stellarator equilibrium code and those of tokamak perturbative 3D equilibrium codes An investigation into the source of the disagreement has led to new insights into the domain of validity of the different equilibrium

calculations, and to a surprising finding concerning the effect of localized screening currents on global properties of the equilibrium solution. The effect of screening currents on the global solution suggests that it may be possible to extract information about localized currents from appropriate measurements of global equilibrium plasma properties.

Three approaches have been pursued to investigate the source of the disagreement between the codes: 1. investigation of the domain of validity of the perturbative calculations; 2. comparison of calculated equilibria for simple model cases; 3. comparison with calculated solutions from other codes. Seven codes participated in the work described in this paper: the perturbative tokamak equilibrium codes IPEC[1] and MARS-F[2], the extended MHD code M3D-C1[3], two stellarator equilibrium codes that assume nested flux surfaces, VMEC[4] and NSTAB[5], and two stellarator equilibrium codes that can handle islands and stochastic regions, HINT2[6] and PIES[7]. In Ref 8, comparisons of linear and nonlinear plasma response models are discussed in terms of differences between dynamic evolution and perturbed equilibrium calculations.

The equilibrium studied corresponds to DIII-D shot 142603, which was part of a series of experiments investigating the stabilization of edge localized modes (ELMs) using an applied nonaxisymmetric field. (ELMs were not suppressed in this shot.) The choice of this particular shot was dictated in part by a desire to allow the participation of the full range of tokamak and stellarator equilibrium codes. The IPEC and MARS-F perturbative equilibrium codes assume that the nonaxisymmetric component of the field is small relative to the axisymmetric component. The nonaxisymmetric field imposed for the purpose of ELM suppression in shot 142603 was of order $\delta B / B \approx 10^{-3}$ at the plasma boundary. Some of the stellarator codes, on the other hand, assume a symmetry property called “stellarator symmetry”. This property, satisfied by all of the large contemporary stellarators, corresponds to invariance under simultaneous reflection in the poloidal and toroidal angles. For an axisymmetric configuration, this symmetry property implies up-down symmetry. To allow the participation of the full range of stellarator equilibrium codes, the shot studied was chosen to have a balanced double-null divertor. The applied nonaxisymmetric fields were even-parity (up-down symmetric) and had a three-fold periodicity in the toroidal angle..

Our investigation of the domain of validity of the perturbative equilibrium calculations has found that the perturbative treatment loses its validity at a surprisingly small perturbation amplitude due to an overlap of flux surfaces in the perturbative solution.[8,9] For the particular equilibrium we study, linearized M3D-C1 calculations find that the perturbative treatment breaks down in virtually the entire pedestal region, where the perturbation amplitude is of order $\delta B / B \approx 10^{-3}$. As discussed in Section 3 of this paper, the perturbative solution does appear to retain its validity further into the plasma interior, and the breakdown of the validity of the perturbative treatment does not appear to be the cause of the disagreement between the codes that we have encountered.

As further discussed in this paper, the source of the disagreement between the codes appears to be a difference in the way that the perturbative codes and VMEC handle localized currents at low

order rational surfaces. The equilibrium solutions from the perturbative codes indicate that the presence of the localized currents is associated with a rippling of the equilibrium flux surfaces on the high field side that is not seen in the VMEC solution. This effect of localized screening currents on the global 3D equilibrium solutions suggests that observations of global properties of the tokamak plasma equilibrium can be used to infer properties of localized currents which are difficult to diagnose directly.

The equilibrium solutions discussed in this paper are all intended to satisfy the MHD equilibrium equations,

$$\nabla p = \frac{1}{c}\mathbf{j}\times\mathbf{B},\ \nabla\times\mathbf{B} = \frac{4\pi}{c}\mathbf{j}. \tag{1.1}$$

Some of the codes include rotation effects in their model, but the plasma velocities are not sufficiently large to significantly affect the force-balance equation. The velocity does affect the screening currents. For those codes that assume nested flux surfaces, there are in principle delta function "screening" currents at the rational surfaces that prevent the appearance of magnetic islands. For the M3D-C1 extended MHD code, persistent equilibrium screening currents can be generated by the induced electric field in the reference frame rotating with the plasma, and these screening currents are affected by the rotation frequency. In running the HINT2 and PIES codes, which also do not assume nested flux surfaces, it is generally assumed that there are no screening currents at the rational surfaces.

The current and pressure profiles for the equilibrium calculations are taken to be those found in an axisymmetric kinetic EFIT equilibrium reconstruction.[10] There is some inaccuracy in the profiles arising from the assumption of axisymmetry in the equilibrium reconstruction. The goal of the investigation described in this paper was to compare codes using a common, realistic equilibrium, and not necessarily to obtain the most accurate possible model of the experimental discharge. Nevertheless, for a perturbation of order $\delta B / B \approx 10^{-3}$ the resulting inaccuracy will be small unless there are significant islands present. The plasma in the shot studied was sawtoothing, and there is some uncertainty in the current profile near the magnetic axis. For this study, the safety factor q was taken to be slightly above 1 at the magnetic axis, and there is also some inaccuracy introduced here. Figure 1 shows the reconstructed pressure, q, density, and current profiles for shot 142603 at 3519 ms, the time slice that we have focused on for our investigation. Fig. 2 shows the corresponding reconstructed rotation and Spitzer resistivity profiles. In solving Eqs. (1.1) with the specified pressure and current profiles, we must also specify the boundary conditions. Most of the equilibrium calculations discussed will be free-boundary equilibrium calculations, and for those calculations the location and currents of the external coils are specified, as well as the boundary condition that the magnetic field go to zero at infinity. For fixed boundary calculations, the boundary conditions will be discussed in the following when the calculations are discussed.

In Section II of this paper, we describe the disagreement between VMEC and the perturbative codes. We address the disagreement by comparing calculated equilibria for simple model cases, and by investigating the domain of validity of the perturbative calculations; In Section III, we discuss equilibrium solutions from other codes, and that will provide additional information on the cause of the disagreement between VMEC and the perturbative codes. Section IV discusses the conclusions emerging from the work described in this paper.

II. Disagreement between the VMEC code and the perturbative 3D equilibrium codes.

Figure 3 shows a comparison between the solutions of VMEC, IPEC and MARS-F for the radial displacement of the perturbed q = 8.5/3 flux surface, relative to the radial location of the unperturbed surface, at the toroidal angle $\phi = 0$. The horizontal coordinate in the figure is the poloidal angle, θ. The "unperturbed" surface for VMEC has been taken to be the surface in the corresponding axisymmetric equilibrium solution having the same value of q. The perturbation on the high field side is much larger in the IPEC and MARS-F solutions than in the VMEC solution. The difference might be expected if the VMEC calculation retained an insufficient number of poloidal modes, or if smoothing had been applied to the VMEC solution. The VMEC calculation retained 25 poloidal modes, more than enough to resolve the structure, and no smoothing has been applied.

The disagreement becomes more pronounced with increasing minor radius of the flux surfaces. Figure 4 shows a comparison of the radial perturbation as a function of poloidal angle for the q=13.5/3 surface as calculated by VMEC and IPEC.

In the remainder of this section, we will address the disagreement by investigating the domain of validity of the perturbative calculations and by comparing calculated equilibria for simple model cases. In the next section we will compare with corresponding 3D equilibrium solutions produced by other codes, and that will provide additional information on the source of the disagreement.

We have found that the perturbative treatment loses its validity at a surprisingly small perturbation amplitude due to an overlap of flux surfaces in the perturbative solution.[8,9] To obtain the condition for overlap of flux surfaces, let ψ denote a radial coordinate that labels the flux surfaces, and consider the displacement along any line of constant θ and ϕ, where θ and ϕ denote the poloidal and toroidal angles, respectively. Let ξ_ψ denote the displacement along this line produced by the nonaxisymmetric perturbation. The perturbed flux surfaces do not overlap along this line if and only if $\psi + \xi_\psi$ is monotonically increasing along this line. It follows that the condition for overlap is $\partial \xi_\psi / \partial \psi < -1$.[8,9] For the solutions of the linearized equilibrium equations, ξ_ψ is linearly proportional to the perturbation amplitude. It follows that if $\partial \xi_\psi / \partial \psi$ is negative anywhere, the perturbed flux surfaces of the linearized solution will overlap when the perturbation amplitude is sufficiently large.

Figure 5 shows an evaluation of the overlap criterion for an equilibrium calculated by the linearized M3D-C1 code for shot 142603. The nonaxisymmetric field in the experiment was produced by 4 kA of current in the DIII-D I-coils. The flux surface displacement calculated from the linearized equilibrium equation predicts overlap of the flux surfaces in the white regions. There is a small region of overlap at each of the rational surfaces. In addition, roughly everything outside of the q = 3.5 surface satisfies the overlap condition, despite the fact that the perturbation amplitude is $\delta B / B \approx 10^{-3}$. This roughly comprises the pedestal region. There also is a region adjacent to the overlap region where the perturbative solution does not predict overlap of flux surfaces but where the linear approximation is nevertheless a poor approximation.

Although the assumption that the perturbative solution has good surfaces breaks down in the overlap region, it is still possible to calculate a perturbed magnetic field in that region. In the overlap region, following the field lines of the field calculated in this way would presumably give either an island or a stochastic region. Could this be a reasonable approximation to the field in that region? Boozer and Pomphrey have looked at the consequences of the breakdown of the linear approximation in the neighborhood of rational surfaces.[11] The localized current in the linear solution does not entirely eliminate island formation at the rational surface. A small island remains, filling the region where the linear approximation breaks down. The residual island is much smaller than the island that would appear in the absence of the localized current, with the island width scaling like $\delta B/B$. They find that the linearized solution for the magnetic field in the region of overlap near the rational surface does not appear to provide useful information. The question remains, however, whether the linearized solution in the region of overlap near the plasma boundary might provide useful information.

Another possible source of the disagreement between VMEC and the perturbative codes emerges from a study of equilibrium solutions for simple model cases.[12] Figure 6 shows a fixed boundary solution produced by the IPEC code for a torus with aspect ratio 10 and approximately circular cross-section. The boundary is a circle perturbed by an m=2, n=1 Fourier component, where m is the poloidal mode number and n is the toroial mode number. The mode numbers have been chosen to resonate with the q = 2 rational surface in the plasma interior. The cylindrical force -free solution is plotted for comparison, and it gives a good approximation to the IPEC large aspect ratio solution. The sharp gradient in the IPEC solution at the q=2 rational surface is associated with a very localized current at that surface.

Comparison with a series of corresponding VMEC large aspect ratio solutions with increasing radial resolution[12] finds that the VMEC solutions look quite different from the IPEC solution, and that the VMEC solutions vary significantly with increasing radial resolution up to the highest resolution used, 1599 radial grid surfaces. As the radial resolution is increased, the gradient at the q = 2 rational surface in the VMEC solution increases, but at 1599 radial grid surfaces the magnitude of the gradient is still much smaller than that seen in IPEC. Examination of the current density in the VMEC solutions[12] finds that it becomes increasingly localized at the

rational surface with increasing radial resolution, but is not well localized even at a resolution of 1599 radial grid surfaces. The half-width of the feature at 1599 radial surfaces is over 10% of the minor radius, or about 200 radial grids. It appears that the VMEC code generally does not have very localized currents at rational surfaces. This then is a second possible source of the disagreement between VMEC and the perturbative equilibrium codes.

We have identified two possible sources for the disagreement between VMEC and the perturbative codes. In the next section we will compare with calculations from other codes to pin down the source of the disagreement.

III. 3D equilibrium solutions produced by the other codes.

Comparison with calculations of the other codes indicates that the source of the disagreement between VMEC and the linear codes is a difference in the handling of localized currents at low order rational surfaces, and that breakdown of the perturbative treatment is not an issue at the q = 8.5/3 surface in the DIII-D equilibrium that is the subject of this paper. We will discuss first the issue of the validity of the perturbative treatment, and then turn to the issue of the localized currents.

It was determined in the previous section that the boundary of the edge region where flux surface overlap is predicted in DIII-D shot 142603 is approximately given by the q = 3.5 surface. The q = 8.5/3 surface is well within this, so that overlap is not an issue there. Nevertheless, the question arises whether the boundary conditions are an issue, given that the perturbative solution is not valid in a substantial region near the plasma edge. To address this, a nonlinear M3D-C1 calculation was compared with a linearized M3D-C1 calculation for the q = 2.42 flux surface, and the result is shown in Fig. 7. The comparison cannot be done at the q = 8.5 / 3 = 2.833 surface, because it is not a good flux surface in the nonlinear M3D-C1 equilibrium solution. The perturbative solution retains screening currents that prevent the q = 8.5/3 surface from breaking up. The question of the possible effect of boundary conditions can be addressed at the q = 2.42 flux surface.

The perturbation amplitude has been scaled up by a factor of 20 in figure 7 to make it visible. There are four surfaces shown. The unperturbed surface and the perturbed surface calculated from the linearized equations are shown, as well as the flux surfaces at $t = 16\mu s$ and $t = 260\mu s$ from a nonlinear M3D-C1 calculation. The nonlinear equilibrium solution is calculated with the M3D-C1 code by following the time evolution of the plasma with the specified boundary conditions until the plasma reaches a steady state. The good agreement between the calculated flux surface shapes at $t = 16\mu s$ and $t = 260\mu s$ indicates that the nonlinear solution has converged.

There is good agreement between the linear and nonlinear solutions in Fig. 7. This indicates that the perturbative treatment does give a valid solution in the region where the perturbation is

sufficiently small that overlap is not an issue, despite the breakdown of the perturbative solution in the pedestal region. In particular, the solution produced by the perturbative codes should be a good approximation to the nonlinear solution at the q=8.5/3 surface. (The perturbative treatment does break down in a very narrow region near the q=8.5/3=17/6 rational surface, but it is a good approximation a short distance away from that surface.)

A linearized M3D-C1 calculation has also been used to look at the effect of the plasma rotation on the equilibrium solution, and this provides information on the effect of localized screening currents at the rational surfaces on the flux surface shape at the q = 8.5/3 surface. The calculated radial displacements for the rotating and nonrotating plasmas are shown in Fig. 8. It is generally believed that screening currents die away rapidly in a non-rotating plasma with non-zero resistivity, but that screening currents persist in a rotating plasma, driven inductively by the $\partial \mathbf{B} / \partial t$ in the reference frame rotating with the plasma. The displacement of the flux surface on the high field side in the M3D-C1 solutions is much smaller in the nonrotating plasma than in the rotating plasma, suggesting that screening currents do play an important role in producing the high field side displacements.

The NSTAB code, like VMEC, assumes nested flux surfaces. It has been shown that NSTAB can handle equilibrium bifurcations involving large localized currents[13], and this suggests that, unlike VMEC, it does retain localized currents at rational surfaces. A free-boundary capability has not been developed for the NSTAB code, and, for its calculation of the equilibrium solution for shot 142603, a fixed boundary calculation was done using the plasma boundary found by VMEC. A plot of the calculated radial displacement of the q=8.5/3 surface as a function of poloidal angle is shown as Fig. 9. Although the solution has been constrained to agree with that of VMEC at the plasma boundary, the amplitude of the calculated displacement on the high field side lies between that of VMEC and those of the perturbative equilibrium codes. This appears to provide further evidence that the source of the disagreement between VMEC and the perturbative codes in the calculated solution at the q=8.5/3 surface lies in the difference in handling localized currents.

Finally, we turn to nonlinear solutions that do not assume nested flux surfaces. Bothe the HINT2 and nonlinear M3D-C1 code find a substantial region of stochastic field lines in the outer region of the plasma. Figure 10 shows a Poincare plot for the HINT2 solution, with a substantial stochastic region adjacent to the plasma boundary, and significant islands in the plasma interior.

There is a large density and temperature gradient in the pedestal region in shot 142603. For a free-boundary calculation that does not assume nested flux surfaces, one can ask whether the neoclassical transport produced by the field line stochasticity in the pedestal region is too large to be consistent with the observed temperature and density gradients. Alternatively one can ask whether it is possible to construct a self-consistent solution in which the inductive electric field in the reference frame of the plasma rotating at the observed frequency maintains screening

currents that prevent the appearance of significant magnetic islands in the pedestal. Those questions are outside the scope of this paper.

The PIES 3D equilibrium code also can handle islands and stochastic regions. The code has been extensively benchmarked, for both fixed-boundary and free-boundary stellarator equilibria, against the VMEC code.[14] When calculating stellarator equilibria, the PIES code assumes that screening currents at rational surfaces do not persist, allowing islands to open. When the island widths and the widths of any stochastic regions are calculated by the PIES code to be small, the solutions produced by the two codes have been found to agree. That is consistent with the findings of this paper. If VMEC is neglecting screening currents, then it could be expected that it would get approximately the same solution as PIES, which is assuming that screening currents are absent, if the islands and stochastic regions in the PIES solution are small. When the PIES solution does have large islands, the VMEC solution does not necessarily provide an indication that the solution with nested flux surfaces is breaking down. This is the case even for vacuum magnetic fields with large islands.[15]

For purposes of comparison with the VMEC code solution for DIII-D shot 142603, a fixed boundary calculation has been done with the PIES code, with the plasma boundary constrained to be the same as that in the VMEC solution. The associated screening currents at the boundary prevent the stochastization of the pedestal region, but screening currents that prevent islands from forming are not present in the plasma interior. If the residual island widths are small in such a calculation, despite the absence of screening currents in the plasma interior, that would suggest that the VMEC fixed boundary solution is self-consistent. Fig. 11 shows the Poincare plot, for the magnetic field that emerges from the PIES fixed-boundary calculation, for a region that extends from $q < 8/3$ to the plasma boundary. The comparison with the VMEC solution has been further facilitated by plotting the PIES solution in VMEC coordinates, so the surfaces would be represented by horizontal lines if they were the same shape as the corresponding VMEC surfaces. Although the constraint at the boundary restricts the size of the magnetic islands, it can be seen that the islands are nevertheless not small, and that they have a significant influence on the shape of the flux surfaces throughout the region shown.

IV. Discussion and conclusions

Three-dimensional equilibrium calculations for DIII-D shot142603 by the VMEC stellarator equilibrium code and by tokamak perturbed equilibrium codes find significantly different solutions on the high field side of the flux surfaces. Investigation of the source of the disagreement has led to an improved understanding of the domain of validity of the codes.

For DIII-D shot 142603, where the magnitude of the nonaxisymmetric perturbation at the plasma boundary is of order $\delta B / B \approx 10^{-3}$, it is found that the perturbative treatment is not valid in the pedestal region due to overlap of the calculated perturbed surfaces[8,9]. Comparison with a nonlinear M3D-C1 solution indicates that the perturbative treatment is valid further into the

interior of the plasma, and that the overlap issue is not responsible for the disagreement between the codes at the q = 8.5/3 surface. (It should be noted that the size of the region near the boundary of the DIII-D plasma where the perturbative treatment breaks down has been found to vary, depending on the specific DIII-D equilibrium studied, and in some shots there is no such region, with the treatment breaking down only near rational surfaces.[9])

Calculations of simple model equilibria indicate that the handling of localized currents at rational surfaces is different in the VMEC code than in the perturbative codes. The evidence suggests that this is the source of disagreement between VMEC and the perturbative codes in our calculations. An M3D-C1 solution for a nonrotating plasma, where screening currents should not persist, gives much better agreement with the VMEC solution than does an M3D-C1 solution for a rotating plasma, where screening currents are expected to persist. The NSTAB code has done a fixed boundary equilibrium calculation where the plasma boundary has been constrained to be the same as that in the VMEC solution, and it nevertheless obtains a solution on the high field side intermediate between that of VMEC and those of the perturbative codes. The calculations of Ref. 13 have indicated that, unlike VMEC, NSTAB does retain localized currents at low order rational surfaces, and this result provides further evidence of the role of localized currents near rational surfaces in contributing to the perturbation on the high field side.

There are two types of localized currents in 3D MHD equilibria. One type is the screening current, which is driven by the inductive electric field in the reference frame moving with a rotating plasma. The second type is the Pfirsch-Schlüter current, which arises from the $\nabla \cdot \mathbf{j} = 0$ constraint on the pressure-driven equilibrium currents. The Pfirsch-Schlüter current should not be significantly affected by a change in the plasma rotation frequency, as long as the plasma velocity is not sufficiently large to affect the force-balance equation. The large difference in the high field side corrugation seen between the rotating and nonrotating M3D-C1 solutions suggests that the corrugation is dominantly produced by the screening current rather than the Pfirsch-Schlüter current.

Theoretical calculations predict that plasma rotation at a rational surface can drive a localized current that screens out resonant perturbations.[16] That does not imply that a 3D equilibrium without significant islands necessarily has localized screening currents. It is possible that the islands at the low order rational surfaces are small because the corresponding resonant components of the magnetic field are small. A PIES calculation finds that, for the DIII-D equilibrium studied in this paper, the island widths are not small relative to the size of the surface displacements being studied, even when the boundary is constrained to be the same as that in the VMEC solution, implying that an equilibrium solution constrained to have good surfaces does have associated screening currents.

The VMEC code has been used extensively for stellarator equilibrium calculations, and that raises the question of the relevance of our findings for stellarator calculations. In the equilibrium for DIII-D shot 142603 discussed in this paper, a resonant perturbation has been imposed with

the intention of breaking flux surfaces in the plasma interior. The presence of the perturbation in a rapidly rotating plasma can lead to the formation of localized screening currents at low order rational surfaces that shield out the resonant components of the perturbation. Stellarator magnetic fields, on the other hand, are designed to have good vacuum flux surfaces, and correspondingly small resonant magnetic field components. After a stellarator device is built, electron beams are used to follow the field lines of the vacuum magnetic field and provide a guide to further tuning of the field, using trim coils to tune out residual islands. Resonant perturbations in the plasma are small at low beta, so that any screening currents at rational surfaces are likely to be small. For a machine such as W7-X, which has been designed to minimize the bootstrap and Pfirsch-Schlüter currents, there is a commensurate reduction in the resonant components of the field driven by finite beta. W7-X, in particular, has low magnetic shear, and the ι (= $1/q$, where q is the safety factor) is adjusted so that rational surfaces in the plasma are of relatively high order. Also, tokamaks can rotate freely in the toroidal direction, and neutral beams can drive strong rotation. That strong rotation, in turn, can drive significant localized currents at rational surfaces that screen out resonant magnetic perturbations. Among stellarators, only quasi-axisymmetric and quasi-helically symmetric configurations can rotate freely.[17] For other stellarators, the neoclassical viscosity plays an important role in determining the plasma flow velocity. These considerations lead to the expectation that localized screening currents generally play less of a role in stellarators than in tokamaks. Nevertheless, localized currents may still play a role, and their potential role is an issue that merits investigation.

Our findings concerning the high field side ripple of the flux surfaces and its relationship to localized screening currents have come from a comparison of 3D equilibrium solutions from seven different codes. Each code has contributed an additional important piece of information to our understanding of this subject.

We have concluded that the significant differences seen between the equilibrium solutions of VMEC and those of the perturbed equilibrium codes for DIII-D shot 142603 are caused by the presence or absence of localized screening currents in the codes. The screening currents themselves are restricted to narrow regions near the low order rational surfaces, and one might have thought that the presence or absence of the screening currents would only lead to differences in the equilibrium solutions in narrow regions near those surfaces. We find that this is not the case, that the effects on the equilibrium are global. An examination of Figures 3 and 4 shows that the response to the external perturbation is significantly affected over a substantial range in poloidal angle, and over a substantial radial range. Unfortunately, the response is largely restricted to the high field side of the tokamak plasma, which is a difficult region for diagnostic access. Our results suggest that diagnostic data relating to the plasma response on the high field side can potentially be a valuable source of information about local properties of the plasma at the low order rational surfaces.

Acknowledgement: This work was supported in part by the U.S. Department of Energy under contracts DE-ACO2-09CH11466, DE-FC02-04E854698, DE-FG02-95E854309, DE-AC05-000R22725 and DE-FG02-86ER53223.

References

[1] J.-K. Park, A. H. Boozer, and A. H. Glasser, Phys. Plasmas **14**, 052110 (2007).

[2] Y. Q. Liu, A. Bondeson, C. M. Fransson, B. Lennartson, C. Breitholtz, Phys. Plasmas **7**, 3681 (2000).

[3] N.M. Ferraro, Phys. Plasmas 19 056105 (2012)

[4] S. P. Hirshman and D. K. Lee, Comput. Phys. Commun. **39**, 161 _1986_.

[5] M. Taylor, J. Comput. Phys., **110**, 407 (1994).

[6] Y. Suzuki, N. Nakajima, K. Watanabe, Y. Nakamura and T. Hayashi, Nucl. Fusion **46**, L19–L24 (2006); K. Harafuji, T. Hayashi, and T. Sato, J. Comput. Phys. **81**, 169 (1989).

[7] A. H. Reiman and H. Greenside, Comput. Phys. Commun. **43**, 157 (1986); D. Monticello, A. Reiman and D. Raburn, Bull. Am. Phys. Soc. **58**, 258 (2013).

[8] A. Turnbull, N. Ferraro *et al*, Phys. Plasmas **20**, 056114 (2013).

[9] Ferraro et al, Nucl. Fusion **53**, 073042 (2013).

[10] L. L. Lao, J. R. Ferron, R. J. Groebner, W. Howl, H. St. John, E. J. Strait, and T. S. Taylor, Nucl. Fusion **30**, 1035 (1990).

[11] A. Boozer and N. Pomphrey, Phys. Plasmas **17**, 110707 (2010).

[12] A. Reiman, T. E. Evans, S. Lazerson *et al*, "A Cross-Benchmarking and Validation Initiative for Tokamak 3D Equilibrium Calculations", TH/P4-7, paper presented at 25th IAEA Int. Conf. on Fusion Energy, St Petersburg, 2014.

[13] P. Garabedian, Proc. Nat. Academy Sci. **103**, 19232 (2006).

[14] J. L. Johnson, D. A. Monticello *et al*, Comput. Phys. Commun. **77**, 1 (1993); A. Reiman, S. Hirshman *et al*, Fus. Sci. and Tech. **51**, 145 (2007).

[15] D. Monticello, M. Mikhailov *et al*, US/Japan JIFT workshop, Princeton, NJ, December 2002, https://docs.google.com/file/d/0B3SxUyX3eGoWWHhHbkxTVXNGNGs/edit

[16] R. Fitzpatrick, Phys. Plasmas **21**, 092513 (2014) and references therein.

[17] P. Helander and A. N. Simakov, Phys. Rev. Lett. 101, 145003.

Figure Captions

Figure 1. The reconstructed pressure, safety factor, density and current profiles for DIII-D discharge 142603 at 3519 ms. from an axisymmetric kinetic EFIT reconstruction.

Figure 2. The reconstructed rotation and Spitzer resistivity profiles for DIII-D discharge 142603 at 3519ms .

Figure 3. Perturbation amplitude (radial displacement) of the q = 8.5/3 surface, relative to the radial location of the unperturbed surface, as a function of the poloidal angle, θ, at $\phi = 0$, as calculated by VMEC, IPEC and MARS-F. ϕ is the toroidal angle. $\theta = 0$ corresponds to the low field side, and $\theta = \pi$ to the high field side.

Figure 4. Perturbation amplitude of the q = 13.5/3 surface as a function of the poloidal angle, θ, at $\phi = 0$, as calculated by VMEC and IPEC.

Figure 5. Contours arising from the evaluation of the overlap condition for an equilibrium calculated by the linearized M3D-C1 code for shot 142603. The flux surfaces are predicted to overlap in the white regions.

Figure 6. IPEC fixed-boundary equilibrium solution for a large aspect ratio torus with nearly circular cross-section. The boundary is a circle with a small n = 1, m =2 perturbation.

Figure 7. Overlay of: the q=2.42 unperturbed flux surface; the q=2.42 surface calculated perturbatively by linearized M3D-C1; the shape of the corresponding flux surface in a nonlinear M3D-C1 calculation at two different times. For each of the nonaxisymmetric surfaces, the perturbation has been scaled up by a factor of 20 to make it visible.

Figure 8. Comparison of linear M3D-C1 solutions for the radial displacement of the q=8.5/3 flux surface with the experimentally determined plasma rotation profile and with no rotation. The displacement of the surface is plotted as a function of the poloidal angle at $\phi = 0$.

Figure 9. Radial displacement as a function of the poloidal angle for an equilibrium generated by the NSTAB code.

Figure 10. Poincare plot of a HINT2 solution for DIII-D shot 142603.

Figure 11. Poincare plot for a region that extends from q < 8/3 to the plasma boundary, for a PIES fixed boundary equilibrium solution with the plasma boundary constrained to be the same as that in the VMEC solution. The solution is plotted in VMEC coordinates, so that the flux surfaces would be horizontal lines if the PIES solution was the same as the VMEC solution. The angular coordinate is the poloidal angle, and the radial coordinate is $\sqrt{s}$, where s is the toroidal flux normalized to its value at the edge.

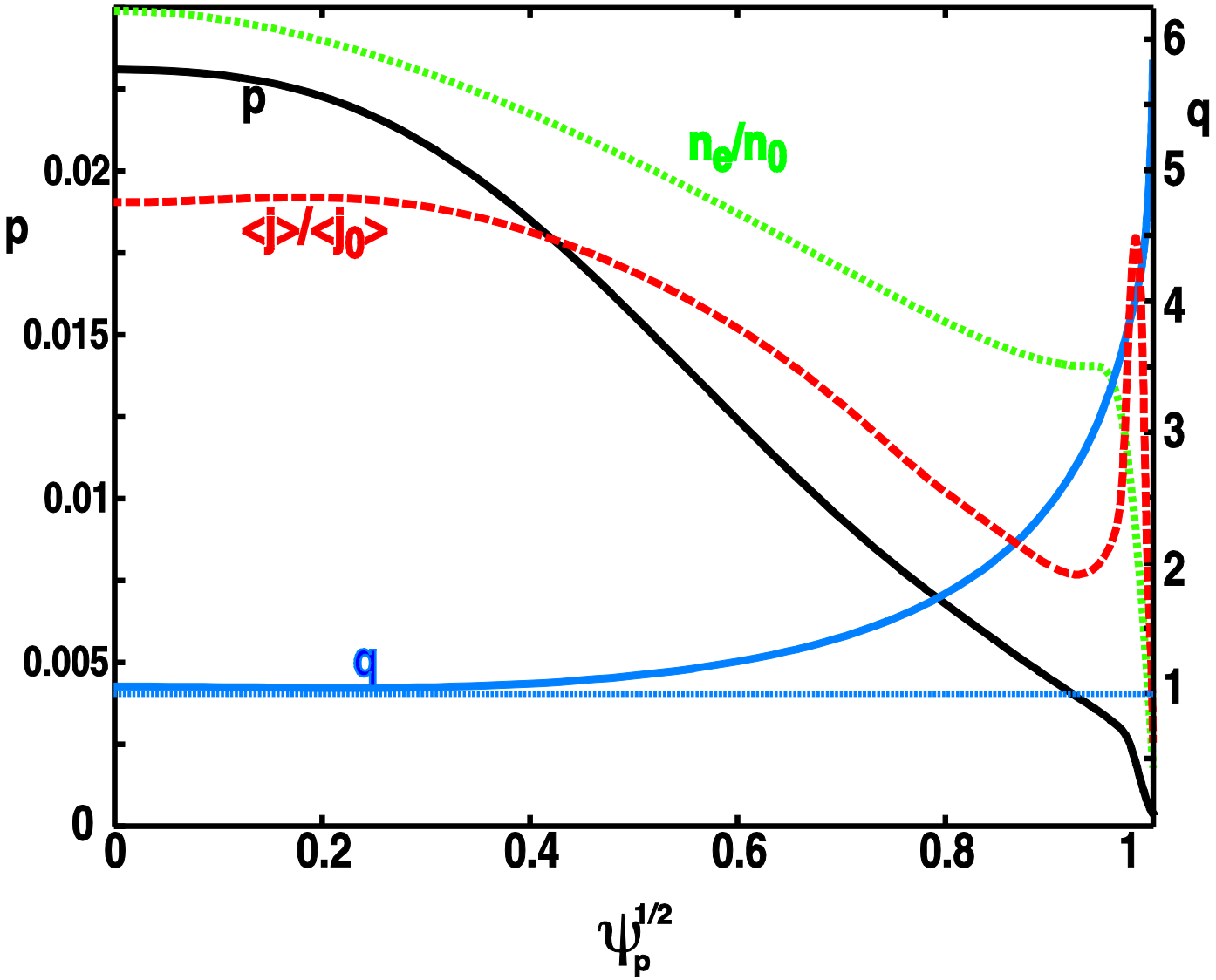
p
q
n_e/n_0
$\langle j \rangle / \langle j_0 \rangle$
q
0.02
0.015
0.01
0.005
0
6
5
4
3
2
1
0
0.2
0.4
0.6
0.8
1
$\psi_p^{1/2}$

Fig. 1

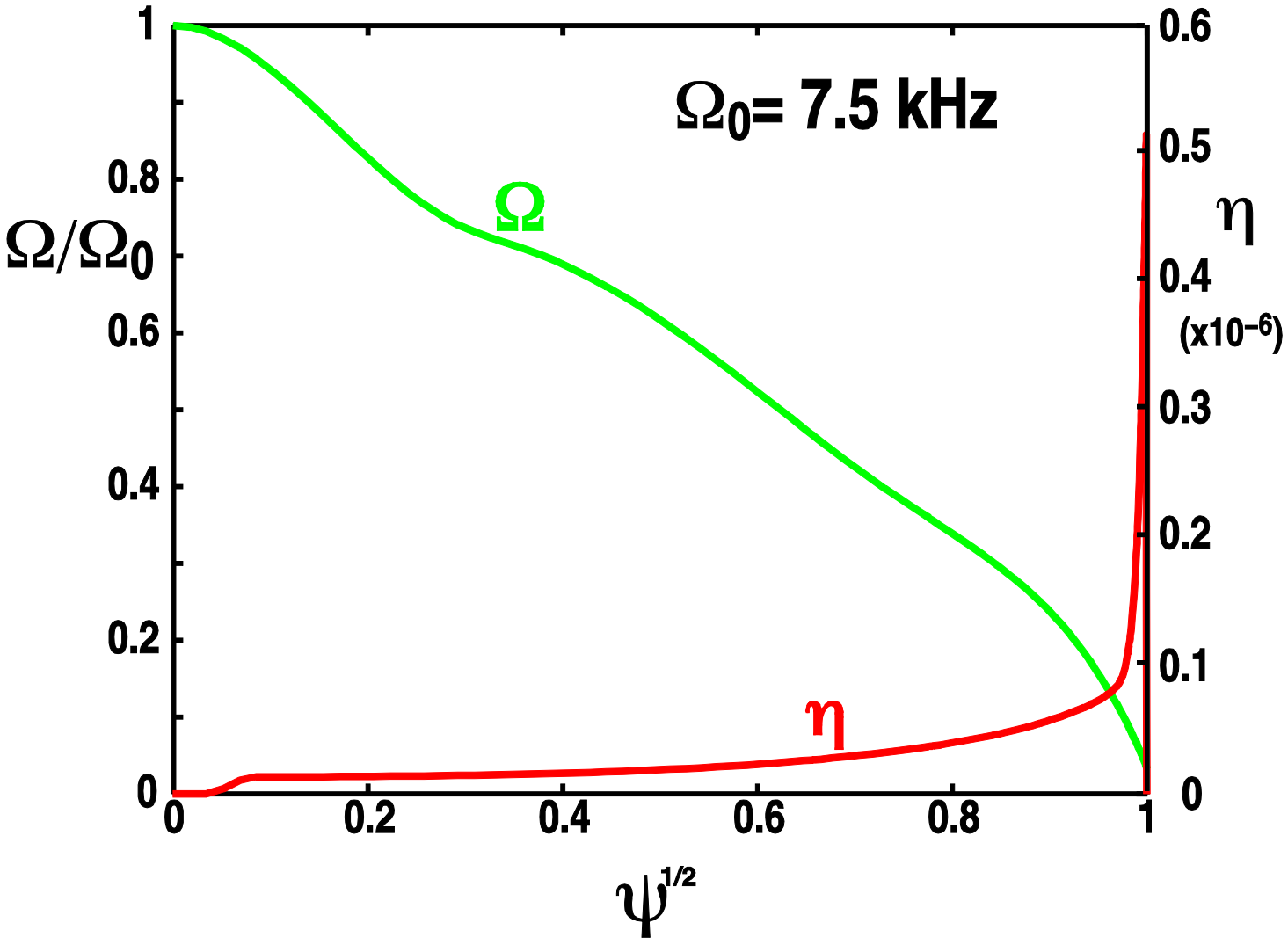
Ω_0= 7.5 kHz
Ω
η
Ω/Ω_0
η
(x10^{-6})
$\psi^{1/2}$
0
0.2
0.4
0.6
0.8
1
0.1
0.3
0.5

Figure 2(

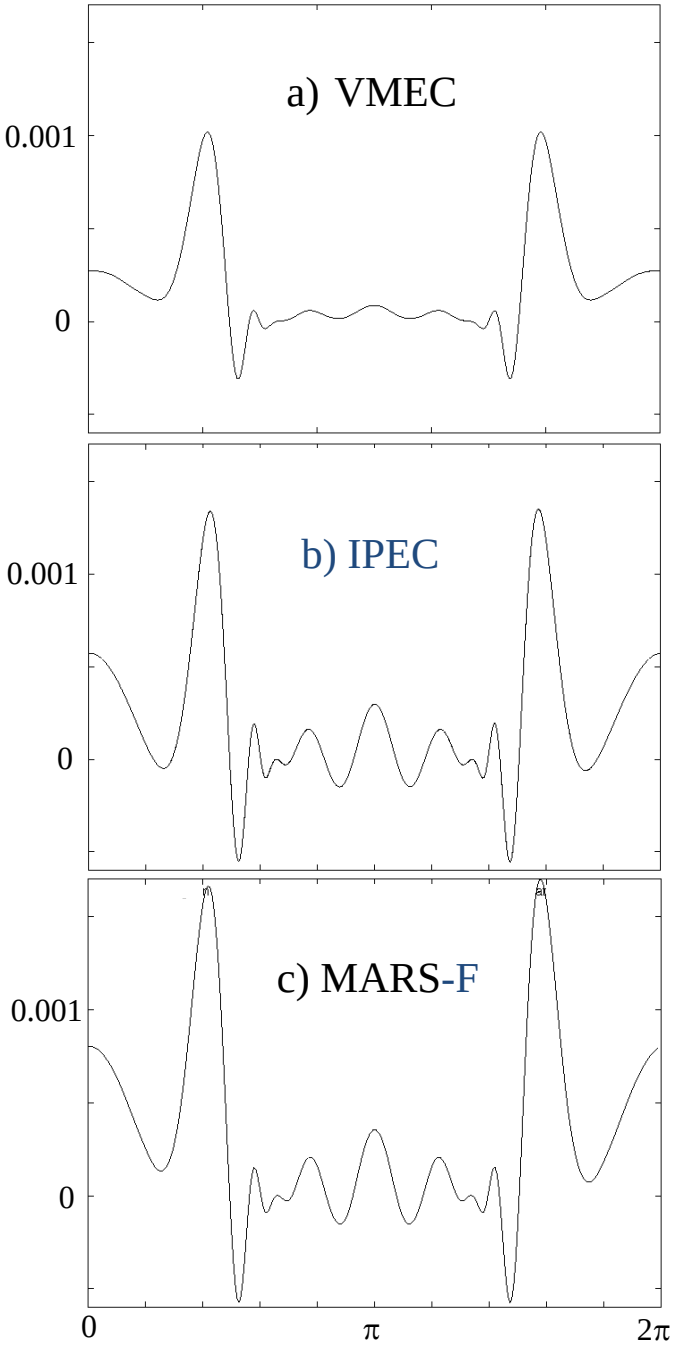

Fig. 3

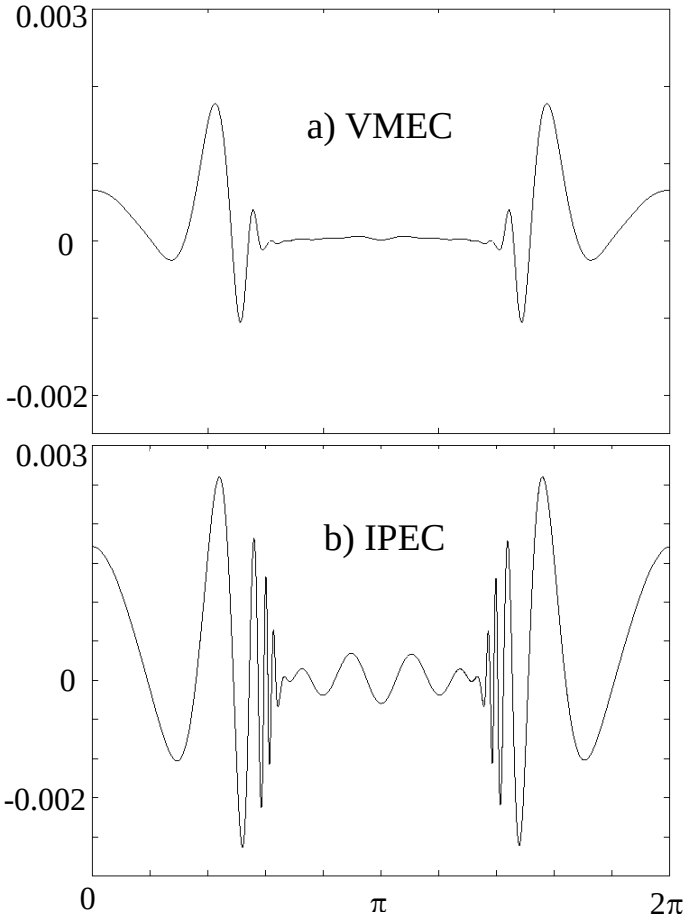

Figure 4

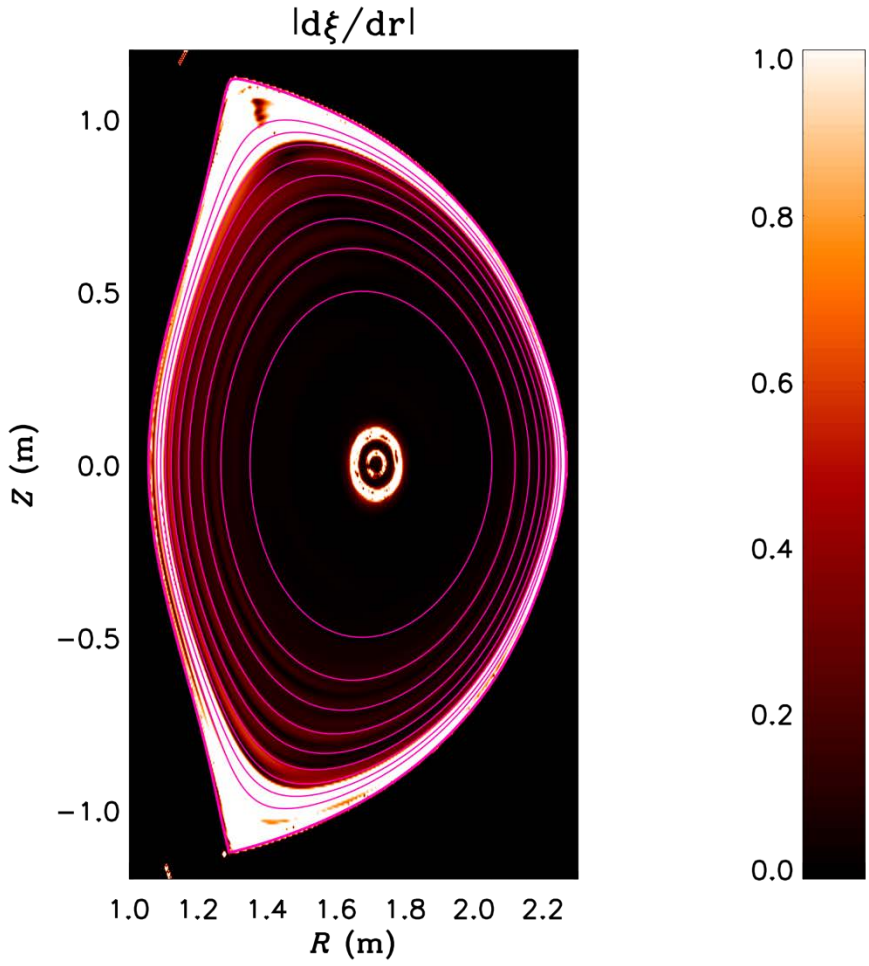

Figure 5

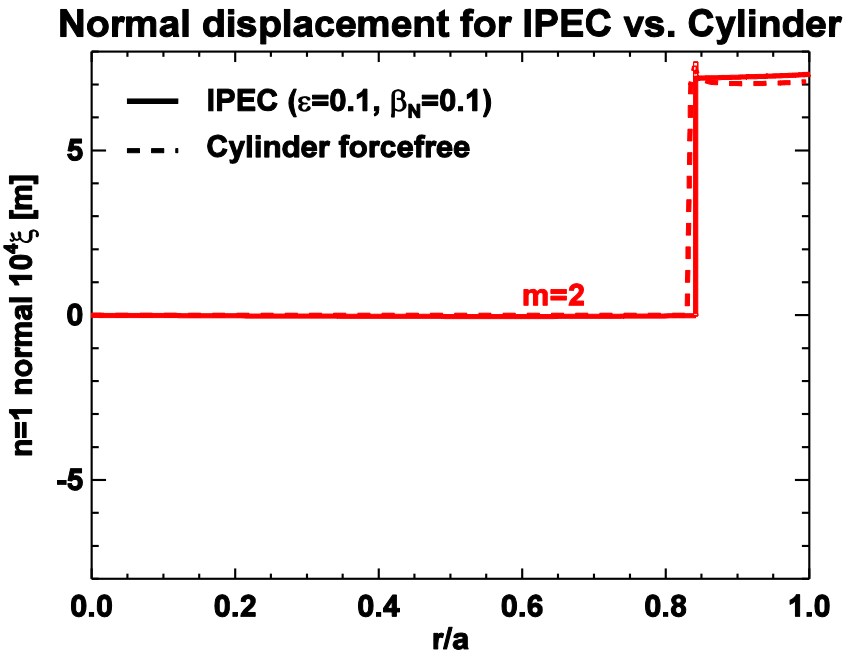
Normal displacement for IPEC vs. Cylinder
IPEC (ε=0.1, βN=0.1)
Cylinder forcefree
m=2
n=1 normal 10⁴ξ [m]
5
0
-5
0.0
0.2
0.4
0.6
0.8
1.0
r/a

Figure 6

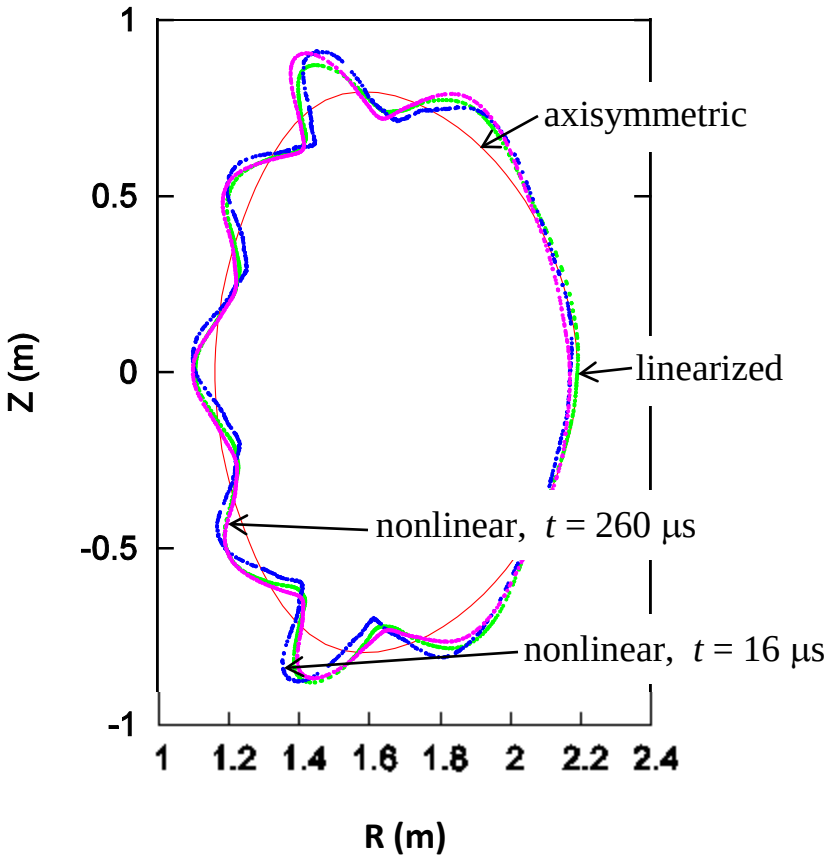
1
0.5
0
-0.5
-1
Z (m)
1
1.2
1.4
1.6
1.8
2
2.2
2.4
R (m)
axisymmetric
linearized
nonlinear, t = 260 μs
nonlinear, t = 16 μs

Figure 7

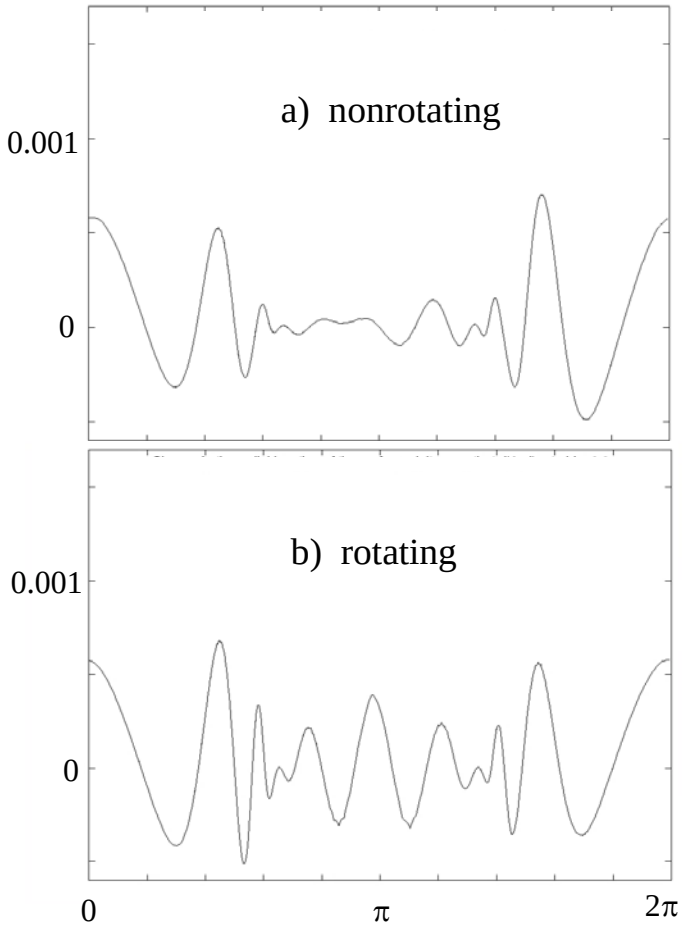

Figure 8

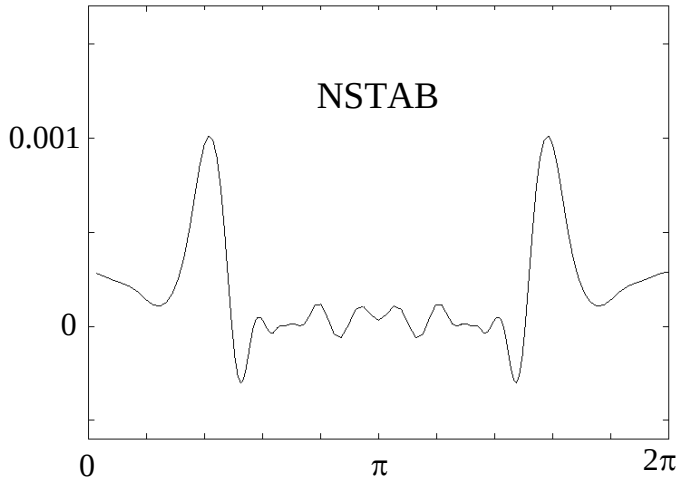

Figure 9

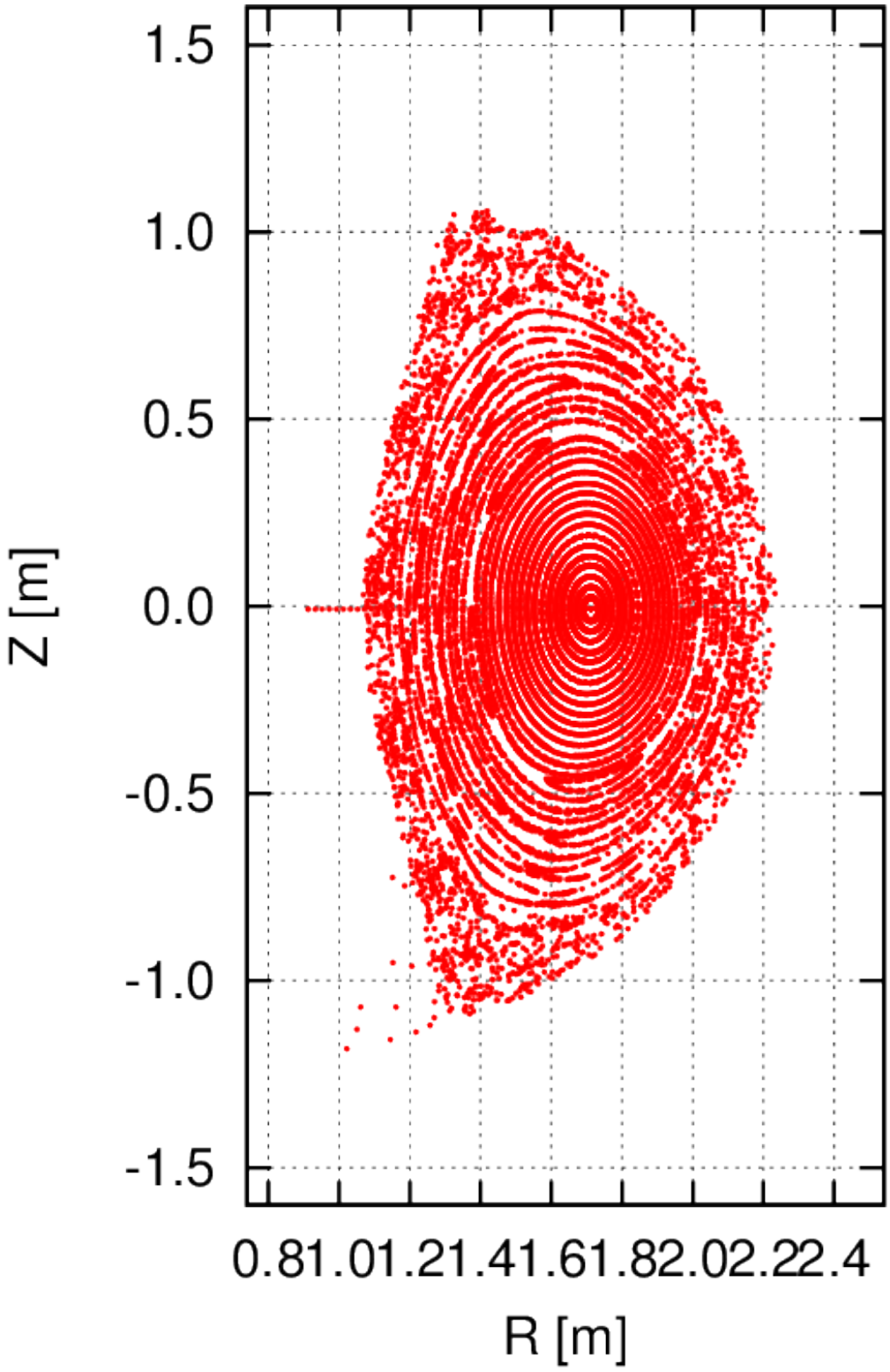

Figure 10

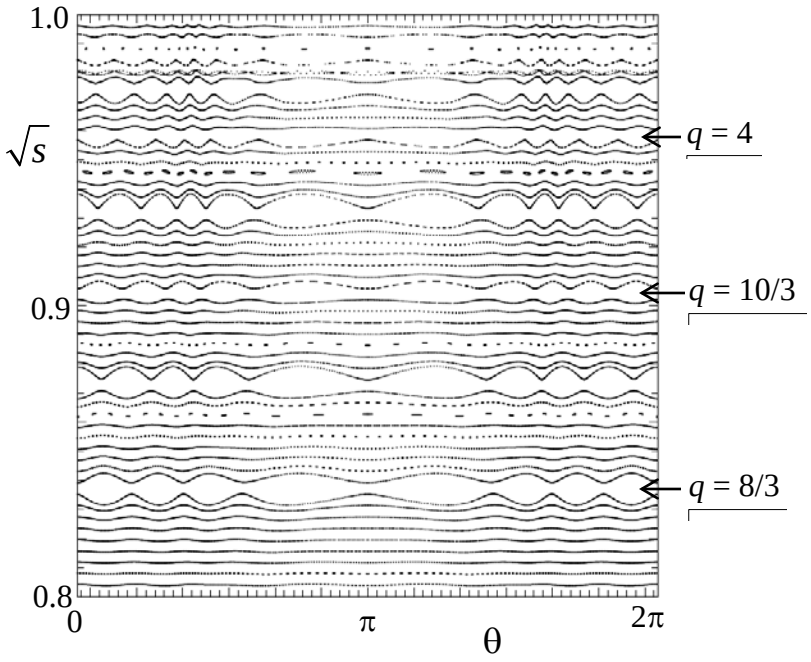

Figure 11